Progress in PHOTOVOLTAICS

PROGRESS IN PHOTOVOLTAICS: RESEARCH AND APPLICATIONS
Prog. Photovolt: Res. Appl. (2013)
Published online in Wiley Online Library (wileyonlinelibrary.com). DOI: 10.1002/pip.2412

RESEARCH ARTICLE

Improved dislocation model of silicon solar cells with the effect of front and back surface recombination velocity

Vinay Budhraja[1,2], Bhushan Sopori[1]*, Nuggehalli Ravindra[2] and Durgamadhab Misra[2]

[1] National Renewable Energy Laboratory, Golden, CO, USA
[2] New Jersey Institute of Technology, Newark, NJ, USA

ABSTRACT

We have extended a previous model for calculating the effects of dislocations on the characteristics of a Si solar cell to include the effects of front and back surface recombination. This improved dislocation model uses Green's function approach to solve the three-dimensional continuity equation of the minority carriers with suitable boundary conditions corresponding to surface recombination at the *n* and *p* sides. The dislocations are considered to be localized lines, extending perpendicular to the front and back surfaces of the cell and having a recombination velocity. We discuss effect of several parameters such as bulk dislocation density, minority carrier diffusion length in *p* and *n* regions on the J-V characteristics, and spectral response of the cell. It is shown that these results agree well with previously published, experimental data.

KEYWORDS
dislocations; Si solar cells

***Correspondence**
Bhushan Sopori, National Renewable Energy Laboratory, Golden, CO, USA.
E-mail: bhushan.sopori@nrel.gov

Received 27 January 2012; Revised 9 January 2013; Accepted 3 July 2013

1. INTRODUCTION

Dislocations and other crystal defects in a wafer are known to have adverse effect on the cell performance, and in the case of multicrystalline silicon (mc-Si), they strongly control the cell efficiency. Most of the studies on the effects of dislocations on the cell performance are carried out experimentally [1–6]. However, it is fruitful to have accurate model to evaluate the effects of dislocations on various cell parameters such as short circuit current density (J_{sc}), open circuit voltage (V_{oc}), and fill factor. In many cases, it is insightful to also determine theoretically the spectral response (SR) of a cell that has a known density of dislocations. Several models were proposed to compute the impact of dislocation density using different approaches. In general, dislocation models are developed for two purposes: (i) to calculate effective minority carrier diffusion length of a semiconductor layer/wafer that can be related to other parameters such as photoluminescence and solar cell parameters [7]; and (ii) directly calculating device characteristics.

Opdorp *et al.* [7] did the theoretical study of the minority carrier recombination at dislocations and calculated carrier distributions within a semiconductor for the case of pulse and sinusoidal excitations. The objective was to relate the measurement of minority carrier lifetime by photoluminescence. The dislocations were considered as cylinders of radius r_0 characterized by a recombination velocity *s*, at the surface of cylinder, and were assumed to be periodically located 2Rs apart in a cylindrical symmetry. The recombination rate was limited by diffusion because the surface recombination velocity was assumed to be large. In the model, the calculations were carried out under the assumption of $s \geq D/r_0$, where *D* is the diffusion coefficient. A simple expression was derived for effective lifetime as a function of dislocation density and then used to determine carrier concentrations under different optical excitation conditions.

Lax [8] applied a similar approach to calculate the effect of dislocation on luminescence intensity of a LED device and showed decrease in electroluminescence efficiency with dislocation density. The dislocations were considered to be perpendicular to the junction. In this model, the surface recombination velocity was taken to finite but assigned large values (i.e., ~10^7 cm/s) in the calculation.

Yamaguchi *et al*. [9] showed the effect of dislocations on cell parameters by solving the one-dimensional continuity equation on *n*±*p* junction. The surface recombination velocities were assumed to be infinity, but the effect of recombination activity at dislocation was not considered. Their calculation results based on one-dimensional model showed a sharp decrease in cell parameters for dislocation densities above $10^5\,cm^{-2}$. Zolper *et al*. [10] used similar model and calculate the effect of dislocations on the open circuit voltage of a solar cell. Moreover, the comparison of measured and modeled values was carried out in their work. The expression of open circuit voltage was derived in the model, which depends on the bulk and dislocation line saturation current densities and surface area of each. In Zolper's model again, the effect of front and back surface recombination velocities were not considered.

Donolato [11] also modeled the effect of dislocations on the minority carrier diffusion length of a semiconductor. He solved the continuity equation in cylindrical coordinates for charge collection probability $\varphi(r)$. The effective diffusion length was solved in the volume integral surrounded by dislocations. In this model, the dislocations were assumed to be line of localized high recombination, S_d. The effect of front surface recombination velocity (S_1) was considered only at the center of dislocation line on front surface, and S_1 was taken same as S_d.

Ghitani *et al*. [12] used a Green's function method to arrive at a numerical solution. For simplicity, the effect of front and back surface recombination velocities was neglected in their model. However, this approximation can cause a significant error, particularly because current mc-Si technology provides surface passivation by SiN:H and very effective back surface fields produced by Al alloying. Furthermore, because there is trend to reduce the wafer thickness below 180 μm, the effects of surfaces can no longer be neglected. In Ghitani model, the effect of emitter was negligible, but in this model, the effect of emitter was considered in the calculations of current densities for the light and dark conditions. In this work, we have extended previous model that uses Green's function approach. Halder *et al*. [13] included the effect of front and back surface recombination velocity in their work, but the model was developed for grain boundaries.

2. THEORY: OUR MODEL

We have considered dislocations in a typical Si solar cell, having an emitter, depletion region, and a base. Furthermore, we have included recombination at both the front and back surfaces. We will use the Green's function approach because it provides an insight into the physical mechanisms. We will follow a formalism similar to that used by Ghitani [12] who ignored the emitter region (as a "dead" layer) and assumed the back recombination to be infinite. It is particularly important to include surface recombination effects because the current Si solar cells have low surface recombination, resulting from SiN:H passivation on the front and back surface field produced by Al alloying on the back. Each dislocation is considered to be a high recombination line perpendicular to the surface and extending through the entire cell.

Our model assumes a uniform distribution of dislocations as shown in Figure 1. The thickness of the cell is *d*. The influence of defects exists in horizontal direction because of dislocation density as well as recombination activity, and the influence of defects exists in vertical direction because of dislocation density as well as front and back surface recombination.

Figure 1 shows the schematic view of *n*±*p* junction, in which the *n*-region exists from $z=0$ to $z=Z_j$, and *p*-region exists from $z=Z_j+W$ to $z=d$. Z_j is the junction depth, W is the width of depletion region, and d is the thickness of the cell.

In the model, we worked on a unit cell, which is surrounded by four dislocations. The dislocations are located on the corners of the cube as shown in Figure 1.

Figure 1 shows the front view of distribution of dislocations. The $z=0$ plane is the top surface of the cell. The carriers can recombine at dislocation from all three dimensions. In this work, the calculations were carried out under following assumptions:

(i) The contribution of emitter was considered.
(ii) Shunt and series resistance effects were neglected.
(iii) The wafer contained a regular array of homogenously recombining dislocations that were perpendicular to the junction area.
(iv) The dislocation was considered to be a space charge cylinder that extends perpendicular from front to back surface of *n*±*p* junction.
(v) The effect of front and back surface recombination velocity was included because the current mc-Si technology provides surface passivation by SiN:H on the front surface and very effective back surface field on the back surface.
(vi) The effect of recombination activity at dislocations was considered.

All these calculations were carried out at the cell thickness of 200 μm. The diffusion length of *p*-region was taken

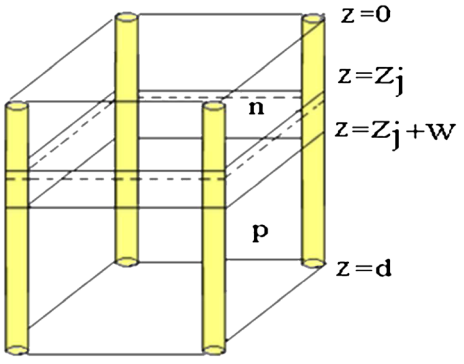

Figure 1. Three-dimensional view of distribution of dislocations, which shows the distribution of dislocations in a unit cell.

to be 400 μm, and the diffusion length of *n*-region was taken to be 10 μm in the calculations.

The distance between two dislocations is 2a. The dislocation density is given by

$$N_d = 1/a^2 \tag{1}$$

In our calculations, the dislocation density was varied from 10^2 to 10^6/cm^2; front and back surface recombination velocities were varied from 10^2 cm/s to infinity.

We used Green's function method to solve the continuity equation for minority carriers in *n* and *p* regions. The detail of the approach to solve the system of equations is discussed in the next section. In this model, the calculations follow a procedure that is previously used by Ghitani *et al*. [12] and Halder *et al*. [13]. We will derive the expressions for the photocurrent generated under air mass (AM)1.5 illumination, dark current as a function of the device voltage, and then use the superposition to arrive at the J-V characteristics of the device.

2.1. Derivations of expressions for the photocurrent under air mass 1.5 illumination

In *n*-region:

The continuity equation to be solved in the *n*-region of the cell is a partial differential equation of the form:

$$\nabla^2(p_n - p_{n0}) - (p_n - p_{n0})/L_p^2 = -\frac{\alpha F(1-R)\, e^{-\alpha z}}{D_p}$$

where the boundary conditions of this upper *n*-region are

$$\frac{\partial(p_n - p_{n0})}{\partial z} = \frac{S_1}{D_p}(p_n - p_{n0}) \quad at \quad z = 0 \tag{3}$$

$$(p_n - p_{n0}) = 0 \quad at \quad z = Z_j \tag{4}$$

$$\frac{\partial(p_n - p_{n0})}{\partial x} = \pm\frac{S_d}{D_p}(p_n - p_{n0}) \quad at \quad x = \pm a \tag{5}$$

$$\frac{\partial(p_n - p_{n0})}{\partial y} = \pm\frac{S_d}{D_p}(p_n - p_{n0}) \quad at \quad y = \pm a \tag{6}$$

Green's function method was used to obtain a solution with the aforementioned boundary conditions. The hole density may be expressed as

$$(p_n - p_{n0})(x', y', z') = < G, f > \tag{7}$$

where the prime variables represent arbitrary points in the volume; the right hand side volume integral is integrated with respect to the unprimed variables *x*, *y*, and *z*. *G* is the symbol for the Green's function, and *f* is defined as

$$f = -\frac{\alpha F(1-R)\, e^{-\alpha z}}{D_p} \tag{8}$$

The Green's function is found by solving the following equation:

$$\nabla^2 G - G/L_p^2 = \delta(x - x')\,\delta(y - y')\,\delta(z - z') \tag{9}$$

with the boundary conditions

$$\frac{\partial G}{\partial z} = \frac{S_1}{D_p} G \quad \text{at} \quad z = 0 \tag{10}$$

$$G = 0 \quad \text{at} \quad z = Z_j \tag{11}$$

$$\frac{\partial G}{\partial x} = \pm\frac{S_d}{D_p} G \quad \text{at} \quad x = \pm a \tag{12}$$

$$\frac{\partial G}{\partial y} = \pm\frac{S_d}{D_p} G \quad \text{at} \quad y = \pm a \tag{13}$$

The solution of equation (9) is expressed by

$$G(x, y, z : x', y', z') = \sum_{m,n}^{\infty} \frac{1}{a^2} \cos(mx)\cos(ny)\; X$$

$$\begin{cases} A\, sinh(z/L_2) + B\, cosh(z/L_2) & if \quad z < z' \\ C\, sinh(z/L_2) + D\, cosh(z/L_2) & if \quad z > z' \end{cases} \tag{14}$$

where

$$1/L_2^2 = n^2 + m^2 + 1/L_p^2$$

The substitution for *G* in boundary conditions given by equations (12) and (13) leads to

$$ma\tan(ma) = -S_d\, a/D_p \tag{15}$$

$$na\, tan(na) = -S_d\, a/D_p \tag{16}$$

The Green's function *G* is continuous at $z = z'$ which leads to

$$G\,(z < z') = G\,(z > z') \quad at \quad z = z' \tag{17}$$

$$\lim_{\epsilon \to 0} \frac{\partial\left(G(z' + \epsilon) - G(z' - \epsilon)\right)}{\partial z} = M_a N_a \cos(mx')\cos(ny') \tag{18}$$

where

$$M_a = m/\left(ma + \left(\frac{1}{2}\right)\sin(2ma)\right)$$

$$N_a = n/\left(na + \left(\frac{1}{2}\right)\sin(2na)\right)$$

We find the values of A, B, C, and D by solving the equations (10), (11), (17), and (18).The excess of minority carriers (holes) is given by the volume integral:

$$\delta p\ (x,y,z) = \int_0^{Z_j}\int_{-a}^{a}\int_{-a}^{a} G f\ dx'dy'dz' \tag{19}$$

$$\begin{aligned}
&= \sum_{m,n}^{\infty} \frac{-4q\alpha F(1-R)\sin(ma)\sin(na)}{mna^2}\left\{A\left[L_2 e^{-\alpha z}\cosh\left(\frac{z}{L_2}\right)\right.\right.\\
&+\alpha L_2^2 e^{-\alpha z}\sinh\left(\frac{z}{L_2}\right) - L_2] + B\left[L_2 e^{-\alpha z}\sinh\left(\frac{z}{L_2}\right)\right.\\
&+\alpha L_2^2 e^{-\alpha z}\cosh\left(\frac{z}{L_2}\right) - \alpha L_2^2] + C\left[\ I_{12} - L_2 e^{-\alpha z}\cosh\left(\frac{z}{L_2}\right)\right.\\
&-\alpha L_2^2 \mathrm{e}^{-\alpha z}\sinh\left(\frac{z}{L_2}\right)] + D\left[I_{11} - L_2 e^{-\alpha z}\sinh\left(\frac{z}{L_2}\right)\right.\\
&\left.\left.\left.-\alpha L_2^2 e^{-\alpha z}\cosh\left(\frac{z}{L_2}\right)]\right\}\cos(\mathrm{mx})\cos(\mathrm{ny})\right.\right.
\end{aligned}$$

The average photocurrent density at a given wavelength is obtained by

$$\begin{aligned}
J_p(\lambda) &= \frac{1}{4a^2}\int_{-a}^{a}\int_{-a}^{a} q\ D_p\left(\frac{\partial \delta p}{\partial z}\right)_{z=Z_j} dx\ dy\\
&= \sum_{m,n}^{\infty} \frac{-4q\alpha F(1-R)M_a N_a \sin^2(ma)\sin^2(na)}{m^2n^2a^2\left(1-\alpha^2L_2^2\right)\left[\frac{1}{L_2}+\frac{S_1}{D_p}\tanh\left(\frac{Z_j}{L_2}\right)\right]}\\
&\left\{\frac{S_1}{D_p}\cosh\left(\frac{Z_j}{L_2}\right)\left[-L_2 + I_{12} - \tanh\left(\frac{Z_j}{L_2}\right)I_{11}\right]\right.\\
&-\alpha L_2\cosh\left(\frac{Z_j}{L_2}\right) + \tanh\left(\frac{Z_j}{L_2}\right)\sinh\left(\frac{Z_j}{L_2}\right)\left[\frac{S_1L_2}{D_p}\right.\\
&\left.+\alpha L_2 - \frac{I_{11}}{L_2}\right] + \frac{I_{12}}{L_2}\sinh\left(\frac{Z_j}{L_2}\right)\\
&\left.+\alpha e^{-\alpha Z_j}\left[L_2 + \tanh\left(\frac{Z_j}{L_2}\right)\frac{S_1L_2^2}{D_p}\right]\right\}
\end{aligned} \tag{20}$$

where

$$I_{11} = L_2\exp(-\alpha Z_j)\sinh\left(\frac{Z_j}{L_2}\right) + \alpha L_2^2\exp(-\alpha Z_j)\cosh\left(\frac{Z_j}{L_2}\right) \text{ and}$$
$$I_{12} = L_2\exp(-\alpha Z_j)\cosh\left(\frac{Z_j}{L_2}\right) + \alpha L_2^2\exp(-\alpha Z_j)\sinh\left(\frac{Z_j}{L_2}\right)$$

In p-region:Similarly, to calculate the photocurrent contribution from the p-region, we now solve the continuity equations for electrons, subjected to the boundary conditions at the edge of depletion region, at the dislocation sites, and at the back contact.

$$\begin{aligned}
&\nabla^2\left(n_\mathrm{p} - n_{\mathrm{p}0}\right) - \left(n_\mathrm{p} - n_{\mathrm{p}0}\right)/L_\mathrm{n}^2\\
&\quad = -\frac{\alpha F(1-R)\ e^{-\alpha z}}{D_\mathrm{n}}
\end{aligned} \tag{21}$$

where the boundary conditions of this lower p-region are

$$\left(n_\mathrm{p} - n_{\mathrm{p}0}\right) = 0 \quad \text{at} \quad z = Z_j + W \tag{22}$$

$$\frac{\partial\left(n_\mathrm{p} - n_{\mathrm{p}0}\right)}{\partial z} = -\frac{S_2}{D_\mathrm{n}}\left(n_\mathrm{p} - n_{\mathrm{p}0}\right) \quad at \quad z = d \tag{23}$$

$$\frac{\partial\left(n_\mathrm{p} - n_{\mathrm{p}0}\right)}{\partial x} = \pm\frac{S_\mathrm{d}}{D_\mathrm{n}}\left(n_\mathrm{p} - n_{\mathrm{p}0}\right) \quad at \quad x = \mp a \tag{24}$$

$$\frac{\partial\left(n_\mathrm{p} - n_{\mathrm{p}0}\right)}{\partial y} = \pm\frac{S_\mathrm{d}}{D_\mathrm{n}}\left(n_\mathrm{p} - n_{\mathrm{p}0}\right) \quad \text{at} \quad y = \mp a \tag{25}$$

The excess of minority carriers (electrons) is given by the volume integral:

$$\begin{aligned}
\delta n(x,y,z) &= \int_{Zj+W}^{d}\int_{-a}^{a}\int_{-a}^{a} Gf\ dx'dy'dz'\\
&= \sum_{m,n}^{\infty}\frac{-4q\alpha F(1-R)\sin(ma)\sin(na)}{mna^2}\\
&\left\{A\left[L_2 e^{-\alpha z}\cosh\left(\frac{z}{L_2}\right) + \alpha L_2^2 e^{-\alpha z}\sinh\left(\frac{z}{L_2}\right) - I_{12}\right]\right.\\
&+B\left[L_2 e^{-\alpha z}\sinh\left(\frac{z}{L_2}\right) + \alpha L_2^2 e^{-\alpha z}\cosh\left(\frac{z}{L_2}\right) - I_{11}\right]\\
&+C\left[I_{222} - L_2 e^{-\alpha z}\cosh\left(\frac{z}{L_2}\right) - \alpha L_2^2 e^{-\alpha z}\sinh\left(\frac{z}{L_2}\right)\right]\\
&\left.+D\left[I_{222} - L_2 e^{-\alpha z}\sinh\left(\frac{z}{L_2}\right) - \alpha L_2^2 e^{-\alpha z}\cosh\left(\frac{z}{L_2}\right)\right]\right\}\\
&\cos(mx)\cos(ny)
\end{aligned} \tag{26}$$

where

$$1/L_2^2 = n^2 + m^2 + 1/L_n^2$$

The average photocurrent density at a given wavelength is obtained by

$$\begin{aligned}
J_\mathrm{p}(\lambda) &= \frac{1}{4a^2}\int_{-a}^{a}\int_{-a}^{a} q\ D_n\left(\frac{\partial \delta n}{\partial z}\right)_{z=Z_j+W} dx\ dy\\
&= \sum_{m,n}^{\infty}\frac{4q\alpha F(1-R)M_a N_a \sin^2(ma)\sin^2(na)}{m^2n^2a^2\left(1-\alpha^2L_2^2\right)\left[\frac{1}{L_2}-\frac{A_1}{L_2A_2}\coth\left(\frac{H}{L_2}\right)\right]}
\end{aligned}$$

$$\begin{aligned}
&\left\{\coth\left(\frac{H}{L_2}\right)\cosh\left(\frac{H}{L_2}\right)\left[\frac{I_j}{L_2} + \frac{A_1 I_{111}}{A_2\ L_2} - \frac{I_{222}}{L_2}\right]\right.\\
&-\frac{I_{11}}{L_2}\cosh\left(\frac{H}{L_2}\right) + \sinh\left(\frac{H}{L_2}\right)\frac{A_1}{A_2}\left[-\frac{I_2}{L_2}\coth\left(\frac{H}{L_2}\right)\right.\\
&+\frac{I_{11}}{L_2} - \frac{I_{111}}{L_2}) + \frac{I_{222}}{L_2}\sinh\left(\frac{H}{L_2}\right)\\
&\left.\left.-\alpha e^{-\alpha H}\left[-L_2 + \frac{A_1}{A_2}\coth\left(\frac{H}{L_2}\right)L_2\right]\right\}\right.
\end{aligned} \tag{27}$$

where

$$H = Z_j + W$$

$$I_{11} = L_2 \exp(-\alpha H) \sinh\left(\frac{H}{L_2}\right) + \alpha L_2^2 \exp(-\alpha H) \cosh\left(\frac{H}{L_2}\right)$$

$$I_{12} = L_2 \exp(-\alpha H) \cosh\left(\frac{H}{L_2}\right) + \alpha L_2^2 \exp(-\alpha H) \sinh\left(\frac{H}{L_2}\right)$$

$$I_{111} = L_2 \exp(-\alpha d) \sinh\left(\frac{d}{L_2}\right) + \alpha L_2^2 \exp(-\alpha d) \cosh\left(\frac{d}{L_2}\right)$$

$$I_{222} = L_2 \exp(-\alpha d) \cosh\left(\frac{d}{L_2}\right) + \alpha L_2^2 \exp(-\alpha d) \sinh\left(\frac{d}{L_2}\right)$$

$$A_1 = \frac{1}{L_2}\cosh\left(\frac{d}{L_2}\right) + \frac{S_2}{D_n}\sinh\left(\frac{d}{L_2}\right)$$

$$A_2 = \frac{1}{L_2}\sinh\left(\frac{d}{L_2}\right) + \frac{S_2}{D_n}\cosh\left(\frac{d}{L_2}\right)$$

In depletion region:The photocurrent collected in the depletion region is [12]

$$J_{dr}(\lambda) = q\,F\,(1-R)\exp\left(-\alpha Z_j\right)\{1 - \exp(-\alpha W)\} \quad (28)$$

The total photocurrent density at a particular wavelength is given by

$$J_{total}\,(\lambda) = J_p(\lambda) + J_n(\lambda) + J_{dr}(\lambda) = J_{sc}(\lambda) \quad (29)$$

The short circuit current density of a solar cell is given by

$$J_{sc} = \int J_{sc}(\lambda)\, d\lambda \quad (30)$$

The absorption coefficient was calculated as [11]

$$\alpha\,(\lambda) = \exp(81.84 - 516.5\,\lambda + 1540\,\lambda^2 - 2421\,\lambda^3 + 2056\,\lambda^4 - 871.4\,\lambda^5 + 135.4\,\lambda^6)\ \mathrm{cm}^{-1}$$

where λ is in micrometer.The SR at different values of wavelength was calculated as

$$SR\,(\lambda) = \frac{J_{sc}(\lambda)}{q\,F(\lambda)} \quad (31)$$

where F is the photon flux at the surface, and its unit is photons-cm^{-2}-s^{-1}. In these calculations, F corresponds to the photon flux for AM 1.5.

2.2. Derivations of expressions for dark current components

In *n*-region: The continuity equation to be solved in the *n*-region of the cell is equation (2) with right hand side equal to zero.

The boundary conditions at $z=0$ and at $x=y=\pm a$ are again given by equations (3), (5), and (6). The boundary condition for hole concentration at the junction is

$$p_n = p_{n0}\exp\left(\frac{qV_j}{kT}\right) \quad at \quad z = Z_j \quad (32)$$

The excess of minority carriers (holes) is given by the surface integral:

$$\delta p\,(x,y,z) = \int_{-a}^{a}\int_{-a}^{a}(p_n - p_{n0})\frac{\partial G}{\partial z}\}_{z=Z_j}\,dx'dy' \quad (33)$$

The average dark current density at a given voltage is obtained by

$$J_p(V_j) = \frac{1}{4a^2}\int_{-a-a}^{a}\int^{a} q\,D_p\left(\frac{\partial \delta p}{\partial z}\right)_{z=Z_j} dx\,dy = \sum_{m,n}^{\infty}\frac{qD_pM_aN_a\sin^2(ma)\sin^2(na)}{m^2n^2a^2}p_{n0}\left\{\exp\left(\frac{qV_j}{kT}\right) - 1\right\}\left\{\frac{\left(\frac{S_1}{D_p}\right)\cosh\left(\frac{Z_j}{L_2}\right) + \left(\frac{1}{L_2}\right)\sinh\left(\frac{Z_j}{L_2}\right)}{\left(\frac{S_1L_2}{D_p}\right)\sinh\left(\frac{Z_j}{L_2}\right) + \cosh\left(\frac{Z_j}{L_2}\right)}\right\} \quad (34)$$

In *p*-region: The continuity equation to be solved in the *p*-region of the cell is a partial differential equation given by equation (21) with right hand side equal to zero.

The boundary conditions at $z=d$ and at $x=y=\mp a$ are again given by equations (23), (24), and (25). The boundary condition for electron concentration at the edge of depletion region is

$$n_p = n_{p0}\exp\left(\frac{qV_j}{kT}\right) \quad \text{at} \quad z = Z_j + W \quad (35)$$

The excess of minority carriers (electrons) is given by the surface integral

$$\delta n\,(x,y,z) = \int_{-a}^{a}\int_{-a}^{a} -\left(n_p - n_{p0}\right)\frac{\partial G}{\partial z}\}_{z=Z_j+W}\,dx'dy' \quad (36)$$

The average dark current density at a given voltage is obtained by

$$J_n(V_j) = \frac{1}{4a^2}\int_{-a}^{a}\int_{-a}^{a} q\, D_n \left(\frac{\partial \delta n}{\partial z}\right)_{z=Z_j+W} dx\, dy$$
$$= \sum_{m,n}^{\infty} \frac{-qD_n M_a N_a \sin^2(ma)\sin^2(na)}{m^2 n^2 a^2} n_{p0} \left\{ \exp\left(\frac{qV_j}{kT}\right) \right.$$
$$\left. -1 \right\} \left\{ \frac{\left(\frac{1}{L_2}\right)\cosh\left(\frac{H}{L_2}\right) - \left(\frac{1}{L_2}\right)\frac{A_1}{A_2}\sinh\left(\frac{H}{L_2}\right)}{\sinh\left(\frac{H}{L_2}\right) - \frac{A_1}{A_2}\cosh\left(\frac{H}{L_2}\right)} \right\} \quad (37)$$

The total dark current density is given by $J_{dark}(V_j) = J_p(V_j) + J_n(V_j)$

The total current density was determined from superposition that is expressed as

$$J_{total}(V_j) = J_{sc} - J_{dark}(V_j) \quad (38)$$

3. RESULTS AND DISCUSSION

3.1. Effect of S_d and N_d

The effect of dislocation density and recombination activity was seen on SR, J-V characteristics, and short circuit current.

Figure 2(a) shows the variation of SR versus wavelength at different values of S_d. The SR shifted downward as the recombination activity increases. The peak of SR photocurrent is shifted toward the longer wavelengths as S_d decreases. When the S_d is low, the recombination rate reduces, which results in an increase in current at all wavelengths. The variation of J-V characteristics is shown in Figure 3(a) at different recombination activities. This figure is plotted by assuming the average dislocation of $10^4\,cm^{-2}$ and finite values of front and back surface recombination velocities.

The short circuit current is calculated from SR values at different wavelengths under the assumption of AM 1.5. The spreadsheet of solar spectral irradiance for AM 1.5

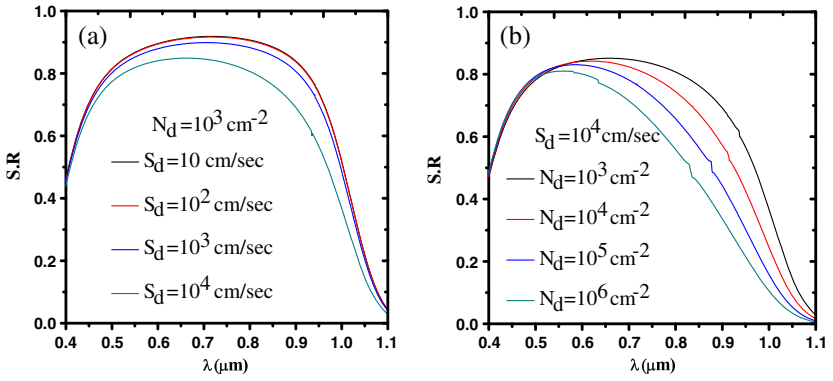

Figure 2. Spectral response versus wavelength of an *n/p* junction with $S_1 = 10^3$ cm/s, $S_2 = 10^4$ cm/s, $Z_j = 0.3\,\mu m$, and $L_n = 400\,\mu m$ (a) for different S_d values ($N_d = 10^3\,cm^{-2}$) and (b) for different N_d values ($S_d = 10^4$ cm/s).

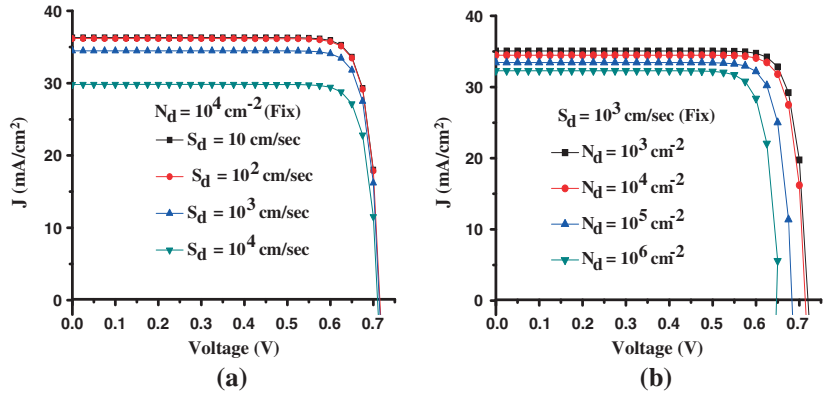

Figure 3. J-V characteristics of an *n/p* junction with $S_1 = 10^3$ cm/s, $S_2 = 10^4$ cm/s, $Z_j = 0.3\,\mu m$, and $L_n = 400\,\mu m$ (a) for different S_d values ($N_d = 10^4\,cm^{-2}$) and (b) for different N_d values ($S_d = 10^3$ cm/s).

gives the power density 1000 W/m^2. All the calculations were carried out at this power density. This spread sheet is provided by the National Renewable Energy Laboratory and available publically [14].

Figure 2(b) shows the variation of SR versus wavelength at different values of N_d, and other parameters such as S_d, S_1, and S_2 are fixed. The peak of SR is shifted toward the longer wavelengths as the dislocation density decreases, and the maximum of SR is shifted toward the shorter wavelengths when N_d increases. There is negligible change in SR with dislocation density at shorter wavelengths. The shorter wavelength (i.e., below 0.4 μm) light has less absorption depth that is why it will penetrate less into the cell and absorbs near the front surface. The change in SR at shorter wavelength is more pronounced with respect to front surface recombination velocity, but at same front surface recombination velocity, there will be very small change in SR at shorter wavelength with respect to N_d and S_d.

The increase in N_d and S_d not only causes a decrease in the maximum value of SR but also shifts the peak of SR toward shorter wavelengths.

Figure 3(b) shows the calculated J-V characteristics at different dislocation densities. The curves of Figure 3(b) indicate as N_d increases; the recombination at dislocations becomes the dominant factor.

3.2. Effect of variation in S_1

Figure 4(a) and (b) shows the variation of SR versus wavelength at different values of S_1. The difference in SR values at different values of S_1 was seen at shorter wavelength. This happens because at shorter wavelength, the absorption depth is low. The light that has the shorter wavelength gives the recombination properties of the front surface as it will absorb near the front surface. SR shifts upward as S_1 decreases because it gives better blue response at lower values of S_1. At longer wavelengths, there is no change in SR values with respect to S_1. This effect can be clearly seen in Figure 4(a) and (b), where the value of SR becomes constant with respect to S_1 at the wavelengths greater than 0.8 μm. At shorter wavelengths, one can clearly see the difference in the curve with respect to S_1.

To see the further effect of S_1, J_{sc} values were plotted at two different dislocation densities. The higher value of J_{sc} was obtained at lower dislocation density and is shown in Figure 5. The change in J_{sc} values is negligible below the S_1 values of 10^4 cm/s and above the S_1 values of 10^8 cm/s. The change in J_{sc} value is more pronounced when S_1 varies from 10^4 to 10^7 cm/s.

3.3. Effect of variation in S_2

Figures 6(a) and (b) shows the variation of SR versus wavelength at different values of S_2. The difference in SR values at different values of S_2 was seen at longer wavelength. This happens because at longer wavelength, the absorption depth is high. The light having longer wavelength gives the recombination properties of the bulk. As the S_2 decreases, the SR shifts upward. At shorter wavelengths, there is no change in SR values with respect to S_2. This effect can be clearly seen in Figure 7(a) and (b), where the value of SR is constant with respect to S_2 below

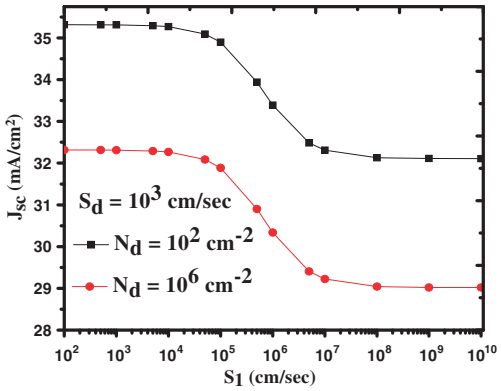

Figure 5. Comparison of J_{sc} values at different dislocation densities with respect to the variation in S_1 when $S_2 = 10^2$ cm/s, $Z_j = 0.3$ μm, and $L_n = 400$ μm.

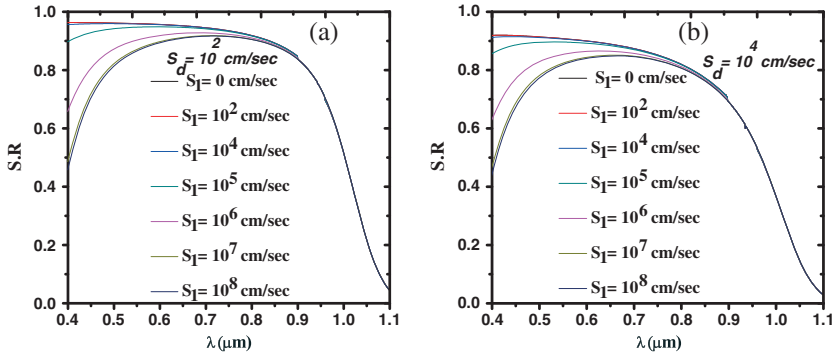

Figure 4. The variation of spectral response versus wavelength at different values of S_1, $N_d = 10^3$ cm^{-2} (fix), $Z_j = 0.3$ μm, and $L_n = 400$ μm for (a) $S_d = 10^2$ cm/s and (b) $S_d = 10^4$ cm/s.

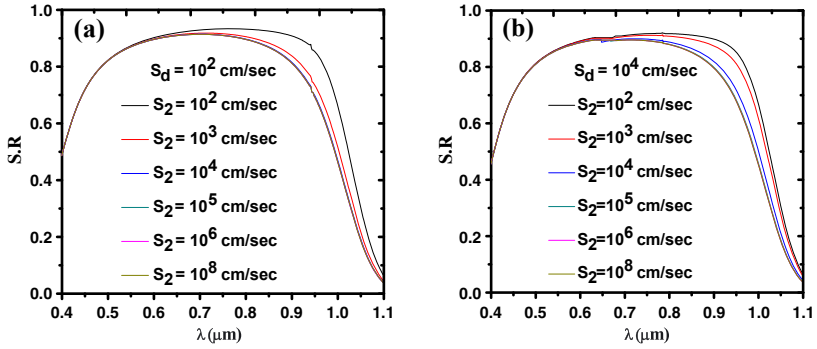

Figure 6. The variation of spectral response versus wavelength at different values of S_2, $N_d = 10^3$ cm^{-2} (fix), $Z_j = 0.3$ μm, and $L_n = 400$ μm for (a) $S_d = 10^2$ cm/s and (b) $S_d = 10^4$ cm/s.

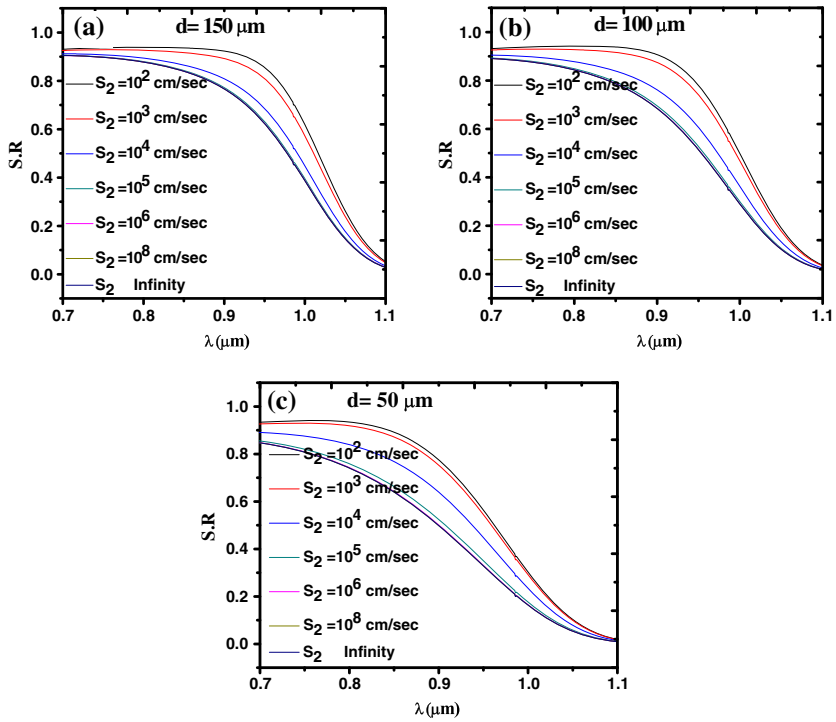

Figure 7. The variation of spectral response with respect to S_2 at longer wavelengths for different thicknesses, $Z_j = 0.3$ μm and $L_n = 400$ μm for (a) $d = 150$ μm, (b) $d = 100$ μm, and (c) $d = 50$ μm.

the wavelength of 0.7 μm. At longer wavelengths, one can clearly see the difference in the curves with respect to S_2.

The change in SR with respect to S_2 will be more pronounce when the thickness of cell is further reduced by the solar industries. This happens because in thinner wafer, the generation rate will be significant at the back surface and no longer be neglected. In Figure 7, the cell thickness was varied from 150 to 50 μm to see the change in SR values with respect to S_2. The difference between the SR values at $S_2 = 10^2$ cm/s, and $S_2 \rightarrow$ infinity increases as the thickness of cell reduces. One can clearly see that the difference between the SR values at $S_2 = 10^2$ cm/s and $S_2 \rightarrow$ infinity is the highest in Figure 7(c), and the difference between the SR values at $S_2 = 10^2$ cm/s and $S_2 \rightarrow$ infinity is the lowest in Figure 7(a).

To see the further effect of S_2, J_{sc} values were plotted at two different dislocation densities. The higher value of J_{sc} was obtained at lower dislocation density and is shown in Figure 8. The change in J_{sc} values is negligible above the S_2 values of 10^6 cm/s. The change in J_{sc} value is more pronounce when S_2 varies from 10^2 to 10^6 cm/s.

3.4. Comparison between modeling and experimental results:

In this model, the effect of S_1 and S_2 is considered, which makes significant difference when it has finite values. The calculated value of short circuit current density at different dislocation densities is shown in Figure 9. The photocurrent

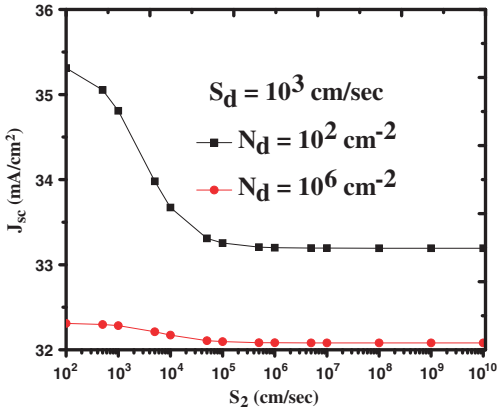

Figure 8. Comparison of J_{sc} values at different dislocation densities with respect to the variation in S_2, when $S_1 = 10^3$ cm/s, $Z_j = 0.3\,\mu$m, and $L_n = 400\,\mu$m.

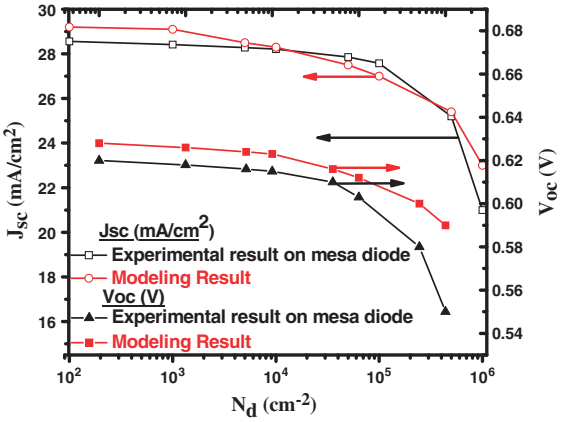

Figure 10. Comparison between modeling and experimental results [15], when $S_1 = 10^5$ cm/s, $S_2 = 10^5$ cm/s, $S_d = 5 \times 10^3$ cm/s, $Z_j = 0.4\,\mu$m, $L_n = 400\,\mu$m, $L_p = 10\,\mu$m, and $d = 250\,\mu$m.

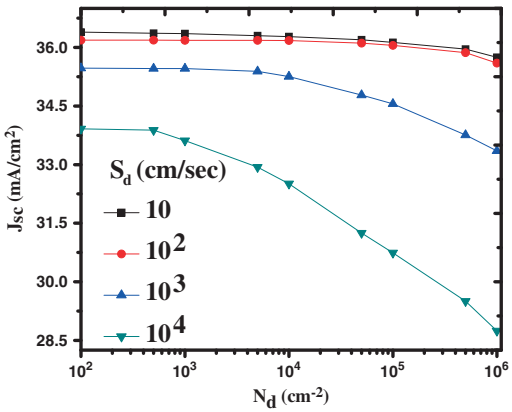

Figure 9. Modeling result: J_{sc} versus N_d at different values of S_d, when $S_1 = 10^3$ cm/s, $S_2 = 10^3$ cm/s, $Z_j = 0.25\,\mu$m, and $L_n = 400\,\mu$m.

decreases as the recombination activity increases at different dislocation densities. All the values of photocurrent were plotted at finite values of front and back surface recombination velocities. At lower values of S_d, the change in J_{sc} is negligible when the dislocation density is below 10^4 cm^{-2}. At higher values of S_d, the change in J_{sc} is negligible when the dislocation density is below 500 cm^{-2}. As the recombination activity increases, the sudden change in J_{sc} will start at low values of dislocation densities.

The modeling results were compared with experimental results reported by Sopori [15]. In his work, he showed the quantitative effect of dislocations on cell parameters using mesa diode arrays [16]. The comparison between these two results is shown in Figure 10. In the comparison, the value of S_1 was taken to be 10^3 cm/s, and the value of S_2 was taken to be 10^4 cm/s.

The experimental results were taken on ribbon sample without antireflective coating. We corrected the experimental data to include the enhancement of J_{sc} (by a factor of 1.4), which gives an excellent agreement between measured and calculated J_{sc} as a function of dislocation density. The correction of V_{oc} involves two features: one due to increase in current and the other due to surface passivation. Because it is difficult to make a correction due to surface passivation, the V_{oc} data have not been corrected, which is the reason of the difference between experimental and modeling values. However, from these comparisons, it is clear that there will be a sudden drop in J_{sc} and V_{oc} values if the dislocation density increases more than 10^4 cm^{-2}. The SR data were not available for comparison with the theory.

3.5. Comparison between modeling values when S_1 and S_2 are considered and neglected:

The J_{sc} and V_{oc} values of our improved model were compared with the Ghitani's model [12] in which the effect of front and back surface recombination velocities was neglected. The comparison between J_{sc} values is given in Table I when S_1 and S_2 are taken to finite, and S_1 and S_2 are neglected or assumed to be infinity. At lower values of S_d, the difference in J_{sc} value increases as N_d decreases; that is, the percentage change in J_{sc} is increasing with decrease in N_d as it is seen in Table I. At high recombination activity, there is a little increase in the percentage change in J_{sc} when N_d decreases from 10^4 to 10^3 cm^{-2}.

Similarly, the comparison between V_{oc} values is given in Table II when S_1 and S_2 are taken to finite, and S_1 and S_2 are neglected or assumed to be infinity. Higher values of J_{sc} and V_{oc} will achieve if surface passivation techniques such as SiN_x:H passivation and back surface field are used in the fabrication of solar cells. In that case, it is important to consider the finite values of front and back surface recombination velocity.

Table I. Change in J_{sc} when S_1 and S_2 are considered and neglected, $Z_j = 0.3\,\mu m$.

S_d (cm/s)	N_d (cm^{-2})	J_{sc} (mA/cm^2) $S_1 = 10^3$ cm/s $S_2 = 10^3$ cm/s	J_{sc} (mA/cm^2) S_1 and S_2 neglected	% change in J_{sc}
10^2	10^5	34.9163	23.9965	45.51
10^2	10^4	35.0644	24.0044	46.07
10^2	10^3	35.7120	24.45	46.08
10^4	10^5	27.9406	20.4759	36.45
10^4	10^4	29.9241	22.4650	33.20
10^4	10^3	31.6754	23.7423	33.41

Table II. Change in V_{oc} when S_1 and S_2 are considered and neglected, $S_d = 10^3$ cm/s.

Z_j (μm)	N_d (cm^{-2})	V_{oc} (V) $S_1 = 10^3$ cm/s $S_2 = 10^3$ cm/s	V_{oc} (V) S_1 and S_2 neglected
0.4	10^5	0.63	0.61
0.4	10^4	0.641	0.62
0.4	10^3	0.652	0.63
0.3	10^5	0.645	0.63
0.3	10^4	0.66	0.645
0.3	10^3	0.68	0.653

4. CONCLUSION

The three-dimensional model of dislocations was developed using Green's function with an effect of front and back surface recombination velocity. In the model, we considered the uniform distribution of dislocations, and the influence of defects is considered in all three dimensions. In the model, the current density equations were solved in both light and dark cases.

The results indicate the effect of dislocation density and recombination activity on SR and J-V characteristics. In the model calculations, it was shown that there is an adverse effect of higher values of dislocation density and recombination activity on the performance of solar cell, which is true as expected. From the SR calculation, it was shown that the effect of front surface recombination velocity is more pronounced at shorter wavelengths, and the effect of back surface recombination velocity is more pronounced at longer wavelengths. The shorter wavelength of light gives the recombination properties of front surface, and longer wavelength of light gives the recombination properties of bulk.

The effect of back surface recombination velocity cannot be neglected in the present crystalline silicon solar cell technology because the thickness of silicon wafer is reduced by solar industries to reduce cost. By Ghitani *et al.* [12], it is concluded that the dislocation effect is less marked when the thickness is less than 50 μm. In his model, the back surface recombination velocity was assumed to be infinity. In our results, we showed that the effect of defects are more pronounced especially in back surface recombination velocity when the cell thickness is less than or equal to 50 μm.

The comparison between experimental and modeling results showed some agreement between two results. There is sudden change in the values of J_{sc} and V_{oc} when dislocation density exceeds 10^4 cm^{-2}. The present model can also be used to compare its results from experimental results of solar cells fabricated on silicon and other semiconductor materials having similar features.

There was significant difference observed in the values of J_{sc} and V_{oc} when front and back surface recombination velocities were taken to be finite and when both were considered to be infinity. This clearly shows that the experimental results of the crystalline silicon solar cells made up on large grain size material can be compared with the dislocation model reported in this work.

This model works for the polycrystalline semiconductor materials of large grain size in which the effect of grain boundary is neglected. The extension of the model is possible by considering the uniform distribution of grain boundary and dislocations. Although our model works only for single junction, our model can be extended by solving continuity equation in different regions using same concept of Green's function. Moreover, the effect of p^+ region, which provides back surface field, can also be included.

LIST OF SYMBOLS

a	Half of the distance between two dislocations
D_n	Electron diffusion coefficient
D_p	Hole diffusion coefficient
d	Thickness of solar cell
f	Distribution function
F	Photon flux
G	Green's function
h	Planck's constant
J	Electric current density
J_n	Electron current density
J_p	Hole current density
J_{dark}	Dark current density
J_{sc}	Short circuit current density
k	Boltzmann's constant
L_n	Minority carrier diffusion length of electrons
L_p	Minority carrier diffusion length of holes
n	Electron concentration
N_A	Number of acceptors

N_D	Number of donors
N_d	Dislocation density
n_i	Intrinsic carrier concentration
n_p	Electron concentration in *p*-region
n_{p0}	Electron concentration in *p*-region at equilibrium
p	Hole concentration
p_n	Hole concentration in *n*-region
p_{n0}	Hole concentration in *n*-region at equilibrium
q	Magnitude of a single electric charge
R	Reflection coefficient
Si_3N_4	Silicon nitride
S_1	Front surface recombination velocity
S_2	Back surface recombination velocity
S_d	Recombination activity at dislocation
SR	Spectral Response
T	Temperature
V_{oc}	Open circuit voltage
V_j	Device voltage
W	Width of depletion region
Z_j	Junction depth
η	Efficiency of a solar cell
v_{th}	Thermal velocity
ε_0	Permittivity of free space
ε_r	Relative permittivity
λ	Wavelength
α	Absorption coefficient

REFERENCES

1. Sopori B, Rupnowski P, Shet S, Mehta V, Budhraja V, Johnston S, Call N, Mountinho H, Al-Jassim M, Shaik A, Seacrist M, Carlson D. Performance limitations of mc-Si solar cells caused by defect clusters. *ECS Transactions* 2009; **18**: 1049–1058.
2. Sopori B, Rupnowski P, Shet S, Budhraja V, Call N, Johnston S, Seacrist M, Shi G, Chen J, Deshpande A. Influence of defects and defect distribution in multicrystalline silicon on solar cell performance. *35th IEEE PVSC* 2010; 2233–2237.
3. Benmohamed Z, Remram M. Effect of dislocation density on the efficiency of multicrystalline silicon solar cells. *Materials Science - Poland* 2007; **25**: 243–249.
4. Cousins PJ, Cotter JE. The influence of diffusion-induced dislocations on high efficiency silicon solar cells. *IEEE Transaction on Electron Devices* 2006; **53**: 457–464.
5. Kieliba T, Riepe S, Warta W. Effect of dislocations on open circuit voltage in crystalline silicon solar cells. *Journal of Applied Physics* 2006; **100**: 093708.
6. Pauls KL, Mitchell KW, Chesarek W. The effect of dislocations on the performance of silicon solar cells. *18th IEEE PVSC* 1993; 209–213.
7. C Van Opdorp, Vink AT, Werkhoven C. Minority carrier recombination at surfaces, dislocations and microdefects: evaluation of parameters from near band edge luminescence. *Proceeding of the 6th III-V Symposium St. Louis MO*, 1976 edited by L.F.Eastman, Inst. Phys. Conf. Ser. 33b, pp. 317, (1977).
8. Lax M. Junction current and luminescence near a dislocation or a surface. *Journal of Applied Physics* 1978; **49**: 2796–2810.
9. Yamaguchi M, Yamamoto A, Itoh Y. Effect of dislocation on the efficiency of thin-film GaAs solar cells on Si substrate. *Journal of Applied Physics* 1986; **59**: 1751–1753.
10. Zolper JC, Barnett AM. The effect of dislocations on the open circuit voltage of gallium arsenide solar cell. *IEEE Transactions on Electron Devices* 1990; **37**: 478–484.
11. Donolato C. Modeling the effect of dislocations on the minority carrier diffusion length of a semiconductor. *Journal of Applied Physics* 1998; **84**: 2656–2664.
12. Ghitani HE, Martinuzzi S. Influence of dislocations on electrical properties of large grained polycrystalline silicon cells. I. Model. *Journal of Applied Physics* 1989; **66**: 1717–1722.
13. Halder NC, Williams TR. Grain boundary effects in polycrystalline silicon solar cells. I: solution of the three dimensional diffusion equation by the green's function method. *Solar Cells* 1983; **8**: 201–223.
14. Website: http://rredc.nrel.gov/solar/spectra/am1.5/#about
15. Sopori BL. Crystal defects in RTR ribbons: their characteristics and influence on the ribbon cell performance. *Journal of Crystal Growth* 1987; **82**: 228–236.
16. Sopori BL. Fabrication of diode arrays for photovoltaic characterization of silicon substrates. *Applied Physics Letters* 1988; **52**: 1718–1720.